Magnetoelastic and neutron-diffraction studies of Cr-Al-alloy single crystals

A. Baran* and H. L. Alberts
Department of Physics, Rand Afrikaans University, P.O. Box 524, Johannesburg 2000, South Africa

A. M. Strydom
Atomic Energy Corporation of South Africa (Ltd.), Pelindaba, Pretoria, South Africa

P. de V. du Plessis
Department of Physics, Rand Afrikaans University, P.O. Box 524, Johannesburg 2000, South Africa
(Received 12 December 1991)

Both magnetoelastic and neutron-diffraction studies have been performed on Cr-Al single crystals containing 1.2, 1.9, and 2.6 at. % Al. These concentrations lie in a controversial region of the magnetic phase diagram. For the crystals containing 1.2 and 1.9 at. % Al the transition at the Néel point is from a paramagnetic to an incommensurate spin-density-wave (ISDW) state while it is from the paramagnetic to a commensurate (C) SDW state for Cr+2.6 at. % Al. All magnetic transitions are observed as second-order phase changes within our experimental resolution. No ISDW-CSDW transition was observed in any of the crystals, and no evidence was found for the existence of mixed ISDW and CSDW phases in the alloys, as previously predicted. The temperature dependence of the elastic constants is described fairly well by existing thermodynamic models, while the magnetization $M^2(T)/M^2(0)$ of Cr + 1.9 at. % Al and Cr+2.6 at. % Al varies as $[1-\alpha(T/T_N)^2+\delta(T/T_N)^4]$ at $T<T_N$. The values of α and δ compare fairly well with values obtained from magnetovolume data.

I. INTRODUCTION

Chromium is an itinerant-electron antiferromagnet, which undergoes a first-order magnetic phase transition to a static sinusoidal spin-density-wave (SDW) state below the Néel temperature $T_N=312$ K. Neutron-diffraction studies of the magnetic structure[1,2] are interpreted in terms of scattering from different Q domains, each described by a wave vector that belongs to the set $\mathbf{Q}_i=(1-\epsilon)(2\pi/a)\hat{\mathbf{x}}_i$, where $\hat{\mathbf{x}}_i$ are unit vectors along the cubic axes of length a. The parameter ϵ is temperature dependent and close to zero, thus describing an incommensurate SDW (ISDW) in the conduction-electron gas. Below T_N the ISDW is transversely polarized with respect to Q, down to the spin-flip temperature $T_{sf}=123$ K, below which the longitudinally polarized ISDW phase appears. Many physical properties were measured in order to investigate these magnetic phase transitions in pure Cr (for a review see Ref. 2). The characteristics of the SDW in Cr are believed to result from nesting between electron and hole sheets in the Fermi surface of the metal. By dissolving other metals in Cr one can change the electron-to-atom ratio, which in turn changes the Fermi surface and thus many physical properties. Alloying Cr with elements that decrease the electron-to-atom ratio normally reduces both the Néel temperature and the wave vector, whereas alloying with elements that increase the electron-to-atom ratio results in increasing the Néel temperature and the wave vector. Cr-Al alloys prove to be an exception: T_N initially decreases with Al addition (up to 1 or 2 at. % Al), but with further increase in Al concentration T_N increases. This gives rise to a minimum in T_N, but as is evident from the results indicated in Fig. 1, there is no quantitative agreement in the literature concerning the position and depth of the minimum as established from electrical resistivity (ρ),[3-8] magnetic susceptibility (χ),[8,9] and magnetoelastic[10,11] studies. Most notable is that Alberts and co-workers[6,10,11] and Sousa *et al.*[8] observed the dip as more pronounced and occurring at a higher Al concentration than Chakrabarti and Beck,[4] Arajs and co-workers[3,5] and Yakhmi *et al.*[7] The resistivity anomaly associated with T_N is small and not well defined between 2 and 4 at. % Al (Ref. 6, see also Ref. 7). Consequently bulk modulus and thermal-expansion measurements (on polycrystalline alloys), which are sensitive parameters to detect T_N in Cr and its alloys, were used by Alberts and Lourens[10,11] to supplement the phase diagram as indicated in Fig. 1(a).

Early powder neutron-diffraction work[12] indicated a crossover from an ISDW to a commensurate SDW (CSDW) between 1 and 4 at. % Al and suggested a mixture of these two phases in the intermediate Al-concentration range. Alberts and Lourens[10,11] also suggested from the broadness of the transitions observed for the bulk modulus and the coefficient of thermal expansion near 2 at. % Al, that such a mixture can occur in this region. Alberts[13] further suggested on the basis of the Al-concentration dependence of the magnetic part of the electrical resistivity that the boundary between the ISDW and CSDW phases is given by the dashed line indicated in Fig. 1(a). Yakhmi *et al.*[7] and Lind and Stanford[14] interpreted their results of resistivity and infrared reflectivity experiments, respectively, on the same single-crystal samples as also indicating the coexistence of the

ISDW and CSDW phases.

This paper reports on magnetoelastic and neutron-diffraction studies of Cr-Al single crystals of compositions 1.2, 1.9, and 2.6 at. % Al, thus representing the controversial region on the magnetic phase diagram. Additional points on the phase diagram are thus established by comparing results of indirect measurement (elastic constants) with direct neutron-diffraction measurement of the spin ordering. Furthermore, the neutron-diffraction studies that extended down to 12 K, should give clarification on speculations regarding mixed ISDW-CSDW phases in this region of the phase diagram and on the boundary between incommensurate and commensurate structures. Our studies extend previous single-crystal neutron-diffraction investigations[15,16] and give *inter alia* detailed measurements near T_N in order to characterize the type of magnetic transition. The magnetoelastic results for the Cr+2.6 at. % Al single crystal have already been reported by Alberts,[17] in the temperature range 77–400 K, whereas our magnetoelastic investigation extends down to 4 K.

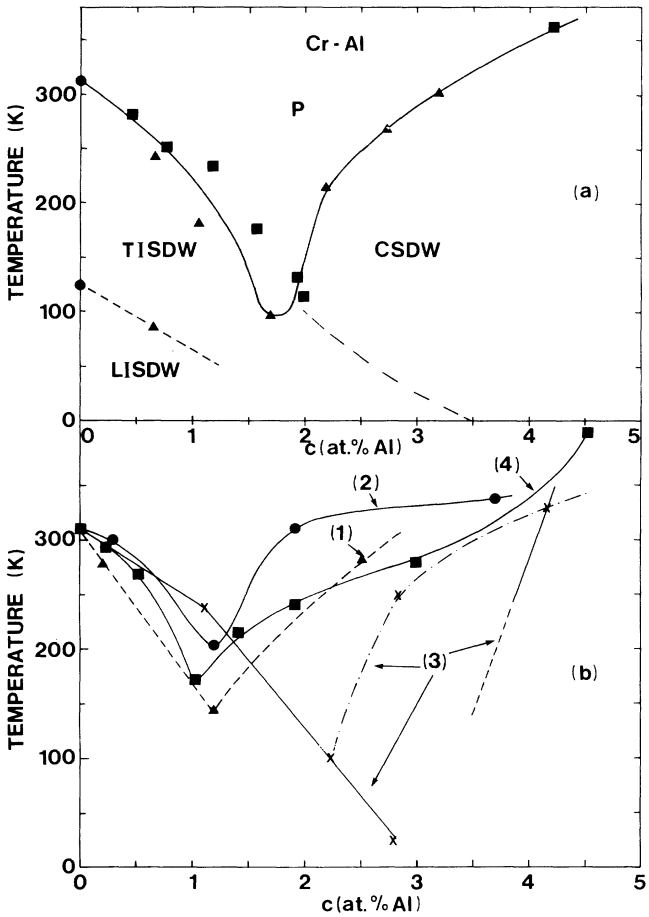

FIG. 1. (a) Magnetic phase diagram of Cr-Al alloys plotted on the basis of previous results of Alberts and co-workers, i.e., electrical resistivity (Ref. 6) (squares) and magnetoelastic data (Refs. 10 and 11) (triangles). The T_N and T_{sf} values for pure Cr (circles) have been taken from Ref. 22. The ISDW-CSDW boundary, marked by the dashed line between points (2 at. % Al, 100 K) and (3.5 at. % Al, 0 K), has been proposed on the basis of the Al-concentration dependence of the magnetic part of the electrical resistivity data for some Cr-Al alloys (Ref. 13). All solid and dashed lines have been drawn as a guide to the eye. (b) Magnetic phase diagram of Cr-Al alloys plotted on the basis of data of Chakrabarti and Beck (Ref. 4) (triangles and line no. 1), data of Arajs and co-workers (Refs. 3 and 5) (circles and line no. 2), data of Sousa *et al.* (Ref. 8) (crosses and line no. 3), and data of Yakhmi *et al.* (Ref. 7) (squares and line no. 4).

The present measurements have been performed on samples in the "multi-Q" state below T_N. The directions of wave vector and spin polarization define six different Q domains for the transverse SDW (TSDW) and three different Q domains for the longitudinal SDW (LSDW). Intuitively one would expect equal volumes of the different domains in the ordered region after cooling a sample slowly through T_N or T_{sf}. Studies on high-purity Cr indicate a considerable hysteresis in the fractional volumes occupied by each of the six types of Q domains comparing scattered neutron intensities obtained from cooling and heating runs.[18] Therefore single-crystal studies are often performed on single-Q specimens prepared as such by cooling through T_N in a magnetic field or with a stress applied along one of the cubic axes.[2] It will be evident from Sec. III that there is little evidence of hysteresis upon thermal cycling in the magnetization curves deduced from neutron scattering and consequently for the present series of experiments, we have been content to study multi-Q samples.

II. EXPERIMENT

Three Cr-Al single crystals with 1.2, 1.9, and 2.6 at. % Al, respectively, have been prepared by a floating-zone method using radio-frequency (rf) heating. Starting materials were polycrystalline rods prepared from 99.996% iochrome and 99.999% pure Al. The final Al concentration for each sample has been determined by electron microprobe analysis. The single crystals containing 1.2 and 1.9 at. % Al were prepared with parallel (100) and (110) faces for ultrasonic measurements by sparking planing, while the crystal containing 2.6 at. % Al was prepared only with parallel (110) faces in order to keep its volume as large as possible for the neutron work. The distances between parallel planes on all the samples were between 5 and 7 mm and the volumes range from 250 to 440 mm^3.

Ultrasonic wave velocities have been measured as a function of temperature using the phase comparison method.[19] X-cut or Y-cut 10-MHz quartz transducers were bonded to the samples with Araldite epoxy resin to generate longitudinal or shear waves, respectively. The experimental error in the absolute values of the wave velocities is estimated to be about 0.5%, while changes of the order of 1 in 10^3 with temperature could be detected easily. The densities of the crystals measured by pycnometric method were used to calculate the elastic constants from the wave velocities. Measurements of wave velocities have been made every 2–3 K. All measurements were done on the as-grown crystals. To check for the effects of strain in the crystals, the Cr+1.9 at. % Al sample was annealed at 1000 °C for 2 h and then furnace cooled. The temperature dependences of the elastic con-

stant $1/2(c_{11}+c_{12}+2c_{44})$ were remeasured and essentially the same results were obtained as on the as-grown crystal, showing that the as-grown crystals are relatively strain free.

Elastic neutron diffraction was employed to obtain magnetization values associated with both the TSDW and the LSDW phases from integrated intensity measurements of magnetic peaks observed in both cooling and heating runs. A monochromatic neutron beam with $\lambda=1.07$ Å was obtained from a (111) plane of a germanium monochromator. The $\lambda/2$ contamination was less than 0.3%. An Euler cradle two-axis diffractometer on which a closed-cycle helium gas cryostat was fitted, was employed. This enabled three-dimensional rotation of the crystal in the neutron beam. Neutron-diffraction patterns were obtained in both ω and $\omega-2\theta$ scanning modes with the [001] axis of the crystal coinciding with the vertical rotation axis of the diffractometer. Data were collected every 0.04° or 0.05° in ω. All measurements were made against a preselected monitor count by using a monitor counter placed in the incoming neutron beam path.

The specimens were secured with Al wire inside an Al can filled with He exchange gas. The can was screwed onto the Cu cold finger of the closed-cycle cryostat, using an In seal for good thermal contact. Temperatures were controlled within ±0.02 K using a GaAs diode as sensor for the proportional temperature controller. Specimen temperatures were measured using two chromel vs Au+0.07 at. % Fe thermocouples fixed at two opposite parts of the sample. These indicated a temperature gradient of less than 0.03 K. An ice triple point cell was employed as temperature reference.

III. RESULTS

A. Results for elastic constants

Ultrasonic velocity measurements along [100] were used to obtain elastic constants c_{11} and c_{44} for longitudinal and shear waves, respectively, while $1/2(c_{11}+c_{12}+2c_{44})$ for longitudinal waves and $1/2(c_{11}-c_{12})$ and c_{44} for shear waves were obtained for propagation along [110]. No corrections were made for changes in the mass density or length of the samples with temperature changes because it follows from thermal-expansion measurements[11] on Cr-Al alloys that such corrections are negligibly small [less than 0.2% in the (4.2–300)-K region] compared to the temperature dependence of the elastic constants.

The temperature dependences of the elastic constants c_{11}, $1/2(c_{11}-c_{12})$, c_{44}, and the bulk modulus $B=1/3(c_{11}+2c_{12})$ are shown in Figs. 2, 3, 4, and 5, respectively (left-hand side plots, solid lines). The dashed lines in the left-hand-side plots of these figures represent the corresponding elastic constants for Cr+5 at. % V alloy.[20] This alloy is ideally suited as a reference material for the nonmagnetic behavior of Cr alloys, since the addition of more than 4 at. % V to Cr destroys the magnetic state in Cr completely without changing either the lattice spacing or mass density by more than 1–2 parts in a thousand.[21] The magnetic contributions to the elastic constants are obtained by subtracting the two curves for each elastic constant and these differences are presented as the solid lines in the right-hand side plots of Figs. 2, 3, and 5. The corresponding Cr+5 at. % V curves were shifted slightly up or down to coincide as closely as possible with the high-temperature data far above T_N, of the Cr-Al alloys. In the case of B the dashed lines of Fig. 5 were determined from the dashed lines of Figs. 2, 3, and 4. The magnetic contribution Δc_{44} was not determined as it is negligible, except near T_{sf} for Cr+1.2 at. % Al, compared to the values

$$\Delta c_{11}\approx 1\times 10^{11}\ \mathrm{N\,m^{-2}}$$

and

$$\Delta[\tfrac{1}{2}(c_{11}-c_{12})]\approx 0.1\times 10^{11}\ \mathrm{N\,m^{-2}}$$

of all three alloys.

The dashed lines indicated on the right-hand side plots of Figs. 2, 3, and 5 represent the best fits of the equation $(1+bT^2+cT^4)$ to experimental results for $T<T_N$ (see discussion in Sec. IV).

Very large magnetic anomalies appear in c_{11} near T_N ($\Delta c_{11}/c_{11}$ of the order of 30%) (Fig. 2) and to a lesser ex-

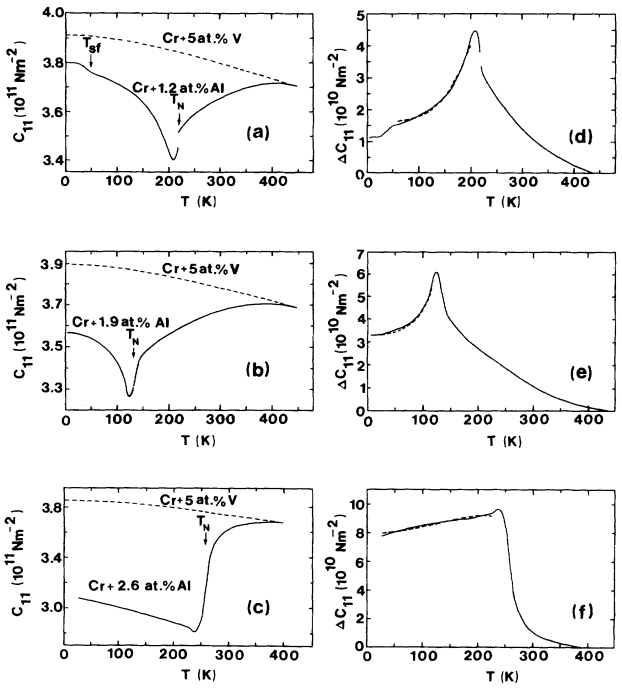

FIG. 2. The temperature dependence of c_{11} and Δc_{11} for Cr-Al single crystals. Solid lines on the left-hand-side figures are smooth curves drawn through the experimental points, which were recorded at about 2-K intervals. The dashed lines on the left-hand-side figures represent c_{11} for Cr+5 at. % V, which represents the nonmagnetic behavior of the antiferromagnetic Cr-Al alloys. The magnetic contribution Δc_{11} was obtained by subtracting the two curves for c_{11} for each alloy. The dashed lines on the right-hand-side figures are the best fits of $\Delta c_{11}(T)/\Delta c_{11}(0)=1+bT^2+cT^4$ to the experimental results.

tent near T_{sf}. The width of the minimum near T_N is much broader than that observed for pure Cr.[22,23] One possible cause for the broader transitions may be sample inhomogeneities. We estimate, however, by comparing the width of the curve near T_N of the Cr+1.2 at. % Al sample with that of pure Cr, that a concentration variation of about 25% of the nominal Al concentration over the sample length is needed to explain the observed broad minimum. This is much larger than the Al-concentration variation estimated by the electron microprobe analysis (about 8%) at different positions on the crystals.

Qualitatively similar λ-type anomalies are observed for c_{11} near T_N for both Cr+1.2 at. % Al and Cr+1.9 at. % Al, while a more jumplike one is observed for Cr+2.6 at. % Al. The λ-type anomaly seems to be characteristic of the paramagnetic (P)-ISDW transition observed by neutron diffraction (see below) in the first two alloys, and the jumplike one of the P-CSDW transition observed for the third concentration. In the case of Cr+1.2 at. % Al [Fig. 2(a)] we observe three characteristic regions for c_{11}: a broad step around 50 K indicating the spin-flip transition from longitudinally to transversally polarized ISDW, verified by neutron-diffraction studies presented below, a minimum at 207 K, and most interestingly, a discontinuous change in c_{11} at 220 K. The discontinuity is accompanied by very large attenuation of the ultrasonic waves in the crystal and may be indicative of a first-order transition. The Néel temperature was taken at the discontinuity for this sample, a choice that is fully supported by the neutron-diffraction data presented below. However, no evidence for a first order transition at T_N is indicated by the neutron-diffraction results.

In the case of Cr+1.9 at. % Al [Fig. 2(b)] there is no trace of a spin-flip transition above 4.2 K. In the region of T_N no discontinuity was observed for this sample but only a minimum at 124 K followed by a kink in the curve occurring to the right of the minimum, at about 143 K. The value of T_N determined from neutron-diffraction experiments on this crystal is equal to 134.2 K, which agrees with the temperature of the inflection point (134 K), occurring between the minimum and the kink in the curve.

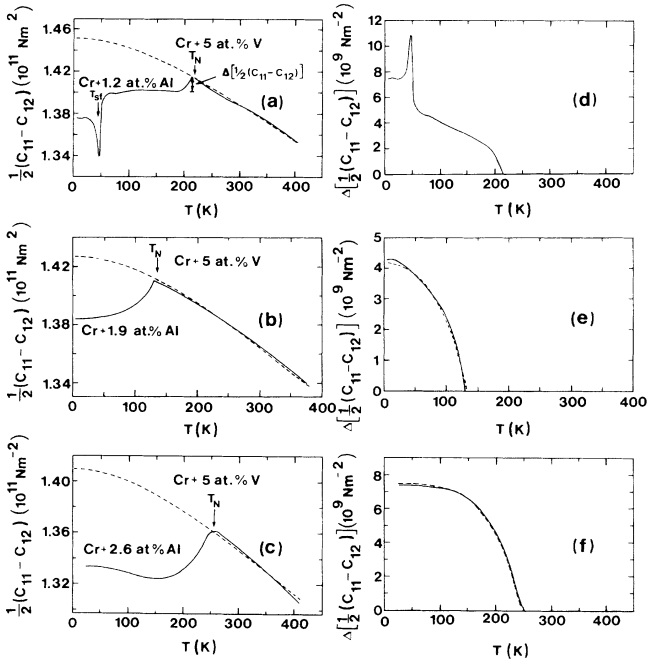

FIG. 3. The temperature dependence of $\frac{1}{2}(c_{11}-c_{12})$ and $\Delta[\frac{1}{2}(c_{11}-c_{12})]$ for Cr-Al single crystals. Solid lines on the left-hand-side figures are smooth curves drawn through the experimental points, which were recorded at about 2-K intervals. The dashed lines on the left-hand-side figures represent $\frac{1}{2}(c_{11}-c_{12})$ for Cr+5 at. % V, which represents the nonmagnetic behavior of the antiferromagnetic Cr-Al alloys. The magnetic contribution $\Delta[\frac{1}{2}(c_{11}-c_{12})]$ was obtained by subtracting the two curves for $\frac{1}{2}(c_{11}-c_{12})$ for each alloy. The small differences of both curves above T_N have been neglected. The dashed lines on the right-hand side figures are the best fits of $\Delta[\frac{1}{2}(c_{11}-c_{12})](T)/\Delta[\frac{1}{2}(c_{11}-c_{12})](0)=1+eT^2+fT^4$ to the experimental results.

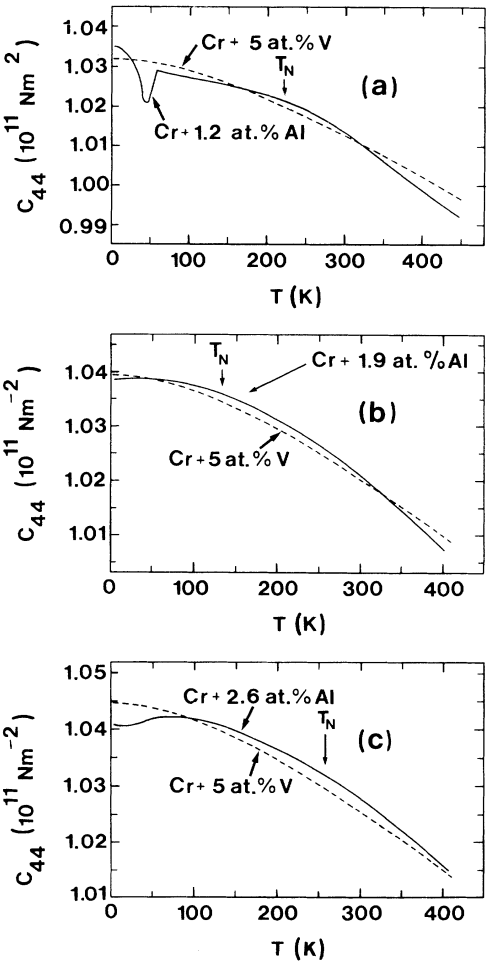

FIG. 4. The temperature dependence of c_{44} and Δc_{44} for Cr-Al single crystals. Solid lines are smooth curves drawn through the experimental points which were recorded at about 2-K intervals. The dashed lines represent c_{44} for Cr+5 at. % V, which represents the nonmagnetic behavior of the antiferromagnetic Cr-Al alloys.

For Cr+2.6 at. % Al the Néel temperature (T_N=256 K) observed with neutron diffraction is in very good agreement with that indicated by the inflection point associated with the jump in c_{11} in Fig. 2(c) (256 K). The magnetic part Δc_{11} (0 K) shown in Figs. 2(d), 2(e), and 2(f) gradually increases as the Al content increases.

Figure 3 shows the temperature variation of $\frac{1}{2}(c_{11}-c_{12})$. For all samples cusplike anomalies are observed near T_N, similarly to that observed in pure Cr.[24] In addition, a relatively deep and sharp anomaly occurs at T_{sf} for Cr+1.2 at. % Al [Fig. 3(a)]. The anomaly in $\frac{1}{2}(c_{11}-c_{12})$ at T_{sf} is much more pronounced than that in c_{11} at the same temperature.

The c_{44} shear constant (Fig. 4) varies within experimental error, smoothly through T_N with little or no magnetic contribution except near T_{sf} for Cr+1.2 at. % Al for which a small but sharp minimum is observed at T_{sf}. The small anomalous behavior of c_{44} for Cr+2.6 at. % Al below 50 K is presently not understood, since the neutron work reported below indicate the existence of a CSDW at all temperatures below T_N for this composition without evidence for a transition to any other magnetic phases.

The temperature variations of the bulk modulus B presented in Fig. 5, resembles qualitatively the corresponding curves of c_{11} (Fig. 2), emphasizing the dominant role of c_{11} in Cr and its alloys.

A point worth mentioning, is the difference in behavior observed for the magnetic effects in the longitudinal constant c_{11} on the one hand and in the shear constants c_{44} and $1/2(c_{11}-c_{12})$, on the other hand. Firstly, magnetic effects persist in c_{11} for Cr-Al to well above T_N, up to as much as 300 K above T_N for Cr+1.9 at. % Al, and secondly, these effects disappear at T_N for $1/2(c_{11}-c_{12})$ and are absent at all temperatures for c_{44}.

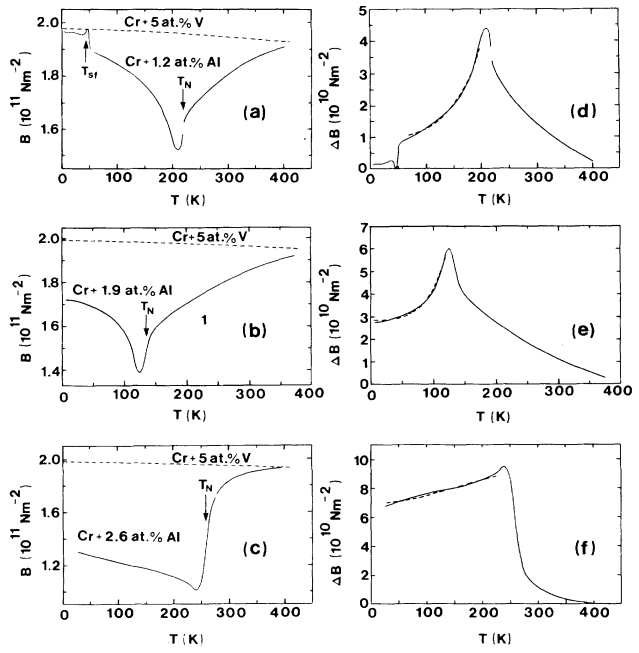

FIG. 5. The temperature dependence of B and ΔB for Cr-Al single crystals. Solid lines on the left-hand-side figures that represent B for Cr-Al alloys were calculated from the corresponding elastic constant curves from Figs. 2, 3, and 4. The dashed lines on the left-hand-side figures that represent B for the Cr+5 at. % V nonmagnetic reference compound were determined from corresponding dashed lines from Figs. 2, 3, and 4. The magnetic contribution ΔB was obtained by subtracting the two curves for B for each alloy. The dashed lines on the right-hand-side figures are the best fits of $\Delta B(T)/\Delta B(0)=1+b_1T^2+c_1T^4$ to the experimental results.

B. Neutron-diffraction results

1. Cr+1.2 at. % Al crystal

The neutron-diffraction patterns for Cr+1.2 at. % Al for three characteristic temperature regions are presented in Fig. 6. The crystal was rotated around the [001] axis through the (010) position using both the ω [Figs. 6(a), 6(b), and 6(c)] and the ω-2θ scanning modes [Fig. 6(d)]. At low temperatures only three magnetic peaks are visible in the ω scan [Fig. 6(a)], two outermost ($\pm\varepsilon$,1,0) satel-

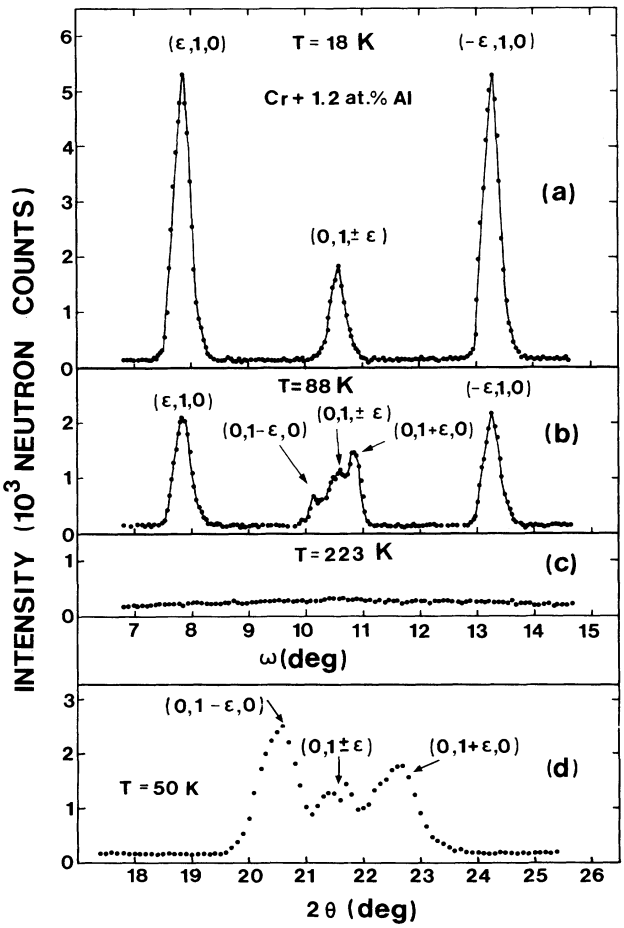

FIG. 6. Neutron-diffraction patterns for Cr+1.2 at. % Al taken through the (010) magnetic position with the [001] axis vertical: (a) ω-scanning mode, $T<T_{sf}$, (b) ω-scanning mode, $T_{sf}<T<T_N$, (c) ω-scanning mode, $T>T_N$, and (d) ω-2θ-scanning mode, $T_{sf}<T<T_N$, central part of the pattern.

lites and the central peak being the superposition of two $(0,1,\pm\varepsilon)$ satellites. This pattern implies that the polarization of the SDW magnetic moments is parallel to the wave vector, like in the case of the low-temperature phase of pure Cr.[25] Above a certain temperature two additional satellites $(0,1\pm\varepsilon,0)$ occur on both sides of the central peak [Fig. 6(b)], indicating that the magnetic moments are polarized perpendicular to the wave vector such as that for pure Cr above the spin-flip temperature.[18] In the critical region just above T_N an almost flat picture with small convexity around the (010) position is observed [Fig. 6(c)]. It was found that the superposition of $(0,1\pm\varepsilon,0)$ and $(0,1,\pm\varepsilon)$ satellites in the central part of Fig. 6(b) could not be resolved better by changing the instrumental parameters in the ω-rotation experiment. The best resolution for these satellites was obtained using an ω-2θ scan as is shown in Fig. 6(d).

The temperature dependences of the $(\varepsilon,1,0)$, $(0,1-\varepsilon,0)$, and $(0,1,\varepsilon)$ satellites have been determined using appropriate scans as indicated in Fig. 6. The results are characteristic of a TSDW below T_N, followed by a transition to a LSDW at temperatures below $T_{sf}\approx 50$ K. Thus we observe that the intensities of both pairs $(\pm\varepsilon,1,0)$ and $(0,1,\pm\varepsilon)$ of satellites increase significantly below T_{sf}, while the intensity of the $(0,1\pm\varepsilon,0)$ satellites falls to zero below T_{sf} for the LSDW.[18,26] The results also show that the Cr+1.2 at. % Al sample remains in the ISDW phase down to the lowest temperature studied (14 K).

Since the $(\varepsilon,1,0)$ satellite in Figs. 6(a) and 6(b) is clearly resolved at all temperatures, a detailed determination of its temperature dependence during cooling and heating runs was performed and the results are depicted in Fig. 7. No hysteresis was observed at T_N. Some small hysteresis effects were observed for results in the ordered region for temperatures below 120 K, but these are small compared with the hysteresis associated with domain effects in pure Cr.[18] A least-squares analysis, presented below in Sec. III B 5, of the detailed measurements, indicated in the inset to Fig. 7, gives $T_N=219.3$ K. This agrees very well with the temperature of the discontinuity in the c_{11} elastic constant of Fig. 2(a) (220 K). No evidence is however found in the neutron-diffraction data of a jump at T_N and consequently the suggestion of a first-order transition from the c_{11} data is not confirmed. It is conceivable, nevertheless, that a smearing effect of a possible discontinuity can occur due to inhomogeneous strain in the sample. In the case of pure Cr, observation of the small first-order phase transition with neutron diffraction was only possible by using very pure and near-perfect single-crystal specimens.[27,28]

Figure 8 shows the temperature dependence of the magnitude Q of the SDW wave vector $\mathbf{Q}=(2\pi/a)(1-\varepsilon,0,0)$. This has been calculated for Cr+1.2 at. % Al independently from the $(\pm\varepsilon,1,0)$ pair of satellites (closed circles) as well as from the $(0,1\pm\varepsilon,0)$ ones (squares). In addition, we present data for Cr+1.9 at. % Al discussed below (crosses) and for pure Cr taken from[18] (triangles). It is interesting to note that the temperature behavior of Q is qualitatively similar in all cases being temperature independent for $T<80$ K and rising sharply for $T>80$ K. Moreover, Q increases with increasing Al content, tending to the CSDW structure ($Q=1$).

2. *Cr+1.9 at. % Al crystal*

For this crystal, neutron scattering indicates a transverse polarization of the ISDW at all temperatures between 14 K and $T_N=134$ K with diffraction patterns qualitatively similar to that of Cr+1.2 at. % Al shown in

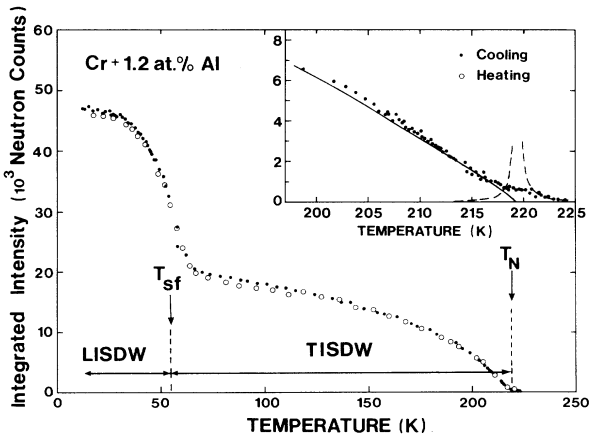

FIG. 7. Temperature dependence of the integrated intensity of the outermost left-hand-side satellite $(\varepsilon,1,0)$ of Fig. 6 for Cr+1.2 at. % Al using the ω-scanning mode. Closed circles denote data collected during a cooling and open circles those collected during a heating run. In the main figure only every tenth point has been displayed in the region of T_N (205–224 K), for clarity. The inset shows the integrated intensity in the vicinity of Néel point. The solid line represents a fit to the data of the magnetization term I_M in Eq. (1) and the dashed lines denote fits of the I_{C+} and I_{C-} critical scattering terms.

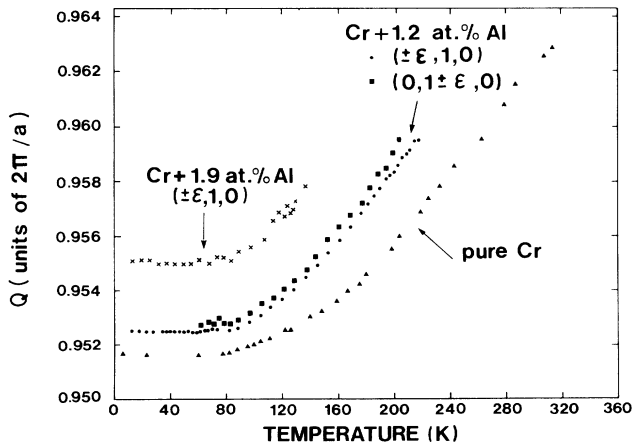

FIG. 8. The temperature dependence of the magnitude of the wave vector $\mathbf{Q}=(2\pi/a)(1-\varepsilon,0,0)$ for Cr-Al single crystals together with data for pure Cr (Ref. 18). Closed circles denote data determined from the $(\pm\varepsilon,1,0)$ satellites and the squares represent values obtained from the $(0,1\pm\varepsilon,0)$ satellites from Fig. 6 for Cr+1.2 at. % Al. The crosses represent the results for Cr+1.9 at. % Al and the triangles data for pure Cr (Ref. 18).

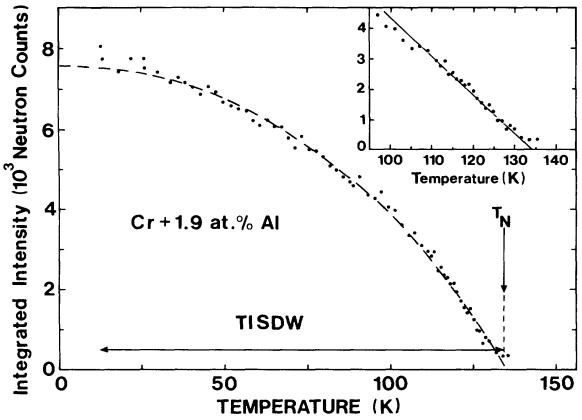

FIG. 9. Temperature dependence of the integrated intensity of the (ε,1,0) satellite measured during a cooling run for Cr+1.9 at. % Al using a ω-scanning mode. The inset shows the integrated intensity in the vicinity of the Néel point. In the inset, the solid-line represents a fit to the data of the magnetization term I_M in Eq. (1). The dashed line in the main figure is the best fit to the data of the equation $M^2(T)/M^2(0)=1-\alpha(T/T_N)^2+\delta(T/T_N)^4$.

Fig. 6(b) or 6(d). No evidence was found from scans with the [001] axis vertical of either a spin-flip transition or of any CSDW-ISDW mixtures. To confirm that there is no contribution coming from the presence of any CSDW phase we changed the configuration of the experiment from the [001] to the [011] vertical rotating axis of the diffractometer and performed ω scans through the (100) position at 14 K. For a pure ISDW phase one does not expect any satellite in the central part of the pattern for the latter configuration, but only the small contribution from the $\lambda/2$ contamination of the neutron beam, (see e.g., Ref. 29). No peak was observed at the (100) position within the resolution of the experiment, thus confirming the absence of the CSDW phase in this alloy.

The temperature dependence of the integrated intensity for the (ε,1,0) satellite measured with an ω scan, is depicted in Fig. 9. No evidence is seen at T_N of a first-order discontinuity in the magnetization and an analysis of the behavior near T_N shown in the inset to Fig. 9, is given in Sec. III B 4. The broken line indicated in the main figure represents the best fit to the data of an equation

$$M^2(T)/M^2(0)=1-\alpha(T/T_N)^2+\delta(T/T_N)^4$$

as is discussed in Sec. IV. The temperature dependence of the magnitude of the **Q** vector for Cr+1.9 at. % Al is presented in Fig. 8 (crosses).

3. Cr+2.6 at. % Al

Results of ω-2θ scans through the (010) position with the [001] axis vertical indicate only a single peak of magnetic origin for this composition between $T_N=256$ and 14 K. This indicates the existence of a simple antiferromagnetic structure commensurate with the crystallographic lattice with wave vector $\mathbf{Q}=(2\pi/a)(1,0,0)$ for Cr+2.6 at. % Al. No sign of a phase transition from CSDW to ISDW or the presence of any ISDW phase was detected in the temperature range used in the experiment. It indicates that the C-I phase boundary presented by Alberts[13] is probably much steeper and shifted towards lower Al concentrations. The Néel temperature determined from a least-squares analysis of the integrated intensity (Sec. III B 5) is equal to 256 K in very good agreement with that determined from the inflection point in the temperature dependence of c_{11}. This points out that the Néel temperature for the Cr+2.83 at. % Al sample, presented by Sousa *et al.*,[8] is rather indicated by the high-temperature anomaly that they observed in both $d\rho/dT$ and $\chi(T)$ in the temperature range $240\leq T\leq 260$ K, and not by the pronounced peak in $\chi(T)$ at 25 K,[8] of which the origin is not clear.

The temperature dependence of the integrated intensity of the (010) magnetic peak is shown in Fig. 10. The transition at T_N seems to be continuous and the critical behavior is analyzed in Sec. III B 5. The dashed line in the main figure is the best fit to the data of the equation

$$M^2(T)/M^2(0)=1-\alpha(T/T_N)^2+\delta(T/T_N)^4$$

as is discussed in Sec. IV.

4. Extinction effects

The integrated neutron intensities plotted in Figs. 7, 9, and 10 are to be used to characterize the temperature dependence of the magnetization both near T_N (Sec. III B 5), as well as down to low temperatures (Sec. IV). Consequently one is concerned whether the measured intensities are affected by extinction. It was not practical with our experimental setup to use a beam of shorter wavelength and thus reduce both the primary and secondary extinctions.[30] Rather, we compared the temperature dependence of the magnetic scattering of the CSDW in the Cr+2.6 at. % Al crystal as measured for the weaker (111) magnetic reflection,[30] with the results given in Fig. 10 as obtained from the stronger (010) reflection. A comparison at the same temperatures of the measured intensities for the (010) and (111) reflections covering the measuring range between T_N and 14 K, is depicted in Fig. 11. The linear relationship in Fig. 11 indicates that even the intensities for the (010) reflection observed at low temperatures, are not adversely affected by extinction. Since the scattered neutron intensity associated with the CSDW structure in Fig. 10 is not expected to be smaller than the (ε,1,0) intensity for either the Cr+1.2 at. % Al crystal in Fig. 7 or the Cr+1.9 at. % Al crystal in Fig. 9, one expects the results reported for the latter two crystals also not to be influenced by extinction.

5. Critical behavior of the Cr-Al crystals

The detailed measurements of integrated magnetic intensity associated with the ISDW in Figs. 7 and 9 and with the CSDW in Fig. 10 near T_N show no evidence of discontinuous behavior or hysteresis effects. Consequently, within the accuracy of our measurements, the transition at T_N can be considered as continuous for all three crystals.

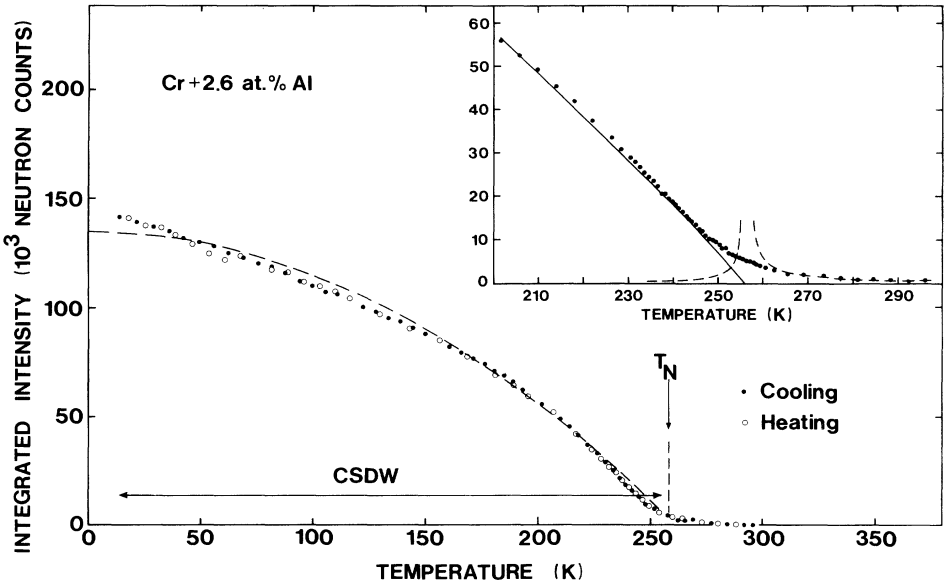

FIG. 10. Temperature dependence of the integrated intensity of the (010) magnetic peak for Cr+2.6 at. % Al using the ω-2θ-scanning mode. Closed circles denote measurements taken during a cooling and the open circles those taken during a heating run. In the main figure every forth point has been displayed in the region of T_N (230–260 K), for clarity. The inset shows the integrated intensity in the vicinity of the Néel point. In the inset, the solid line represents a fit to the data of the magnetization term I_M in Eq. (1) and the dashed lines of the I_{C+} and I_{C-} critical scattering terms. The dashed line in the main figure is the best fit to the data of the equation $M^2(T)/M^2(0)=1-\alpha(T/T_N)^2+\delta(T/T_N)^4$.

Assuming that extinction effects are negligible, it follows that the intensity of the magnetic Bragg reflections $I_M \sim m^2$, where m is the reduced magnetization amplitude, $m=M(T)/M(0)$, associated with the magnetization wave of either incommensurate or commensurate type, as given in Figs. 7, 9, or 10. The spontaneous magnetization near T_N is described in terms of a critical exponent β and the reduced temperature $t_-=(T_N-T)/T_N$ by $m \sim t_-^{\beta}$.[31] In addition, near T_N critical scattering above (I_{C+}) and below (I_{C-}) the Néel point contributes to the measured intensity I:

$$I=I_M+I_{C+}+I_{C-}=Dt_-^{2\beta}+C_+t_+^{-\gamma}+C_-t_-^{-\gamma} . \quad (1)$$

The critical exponent γ is expected by the scaling hypothesis to take on the same value above and below T_N, and $t_+=(T-T_N)/T_N$.[31] The amplitudes C_+ and C_- are related through the parametric representation theory of the equation of state[32]

$$\frac{C_+}{C_-}=\frac{\gamma}{\beta}\left[\frac{(1-2\beta)\gamma}{2(\gamma-1)\beta}\right]^{\gamma-1} . \quad (2)$$

A least-squares fit analysis was made of the experimental data for the Cr+1.2 at. % Al crystal (Fig. 7) and the Cr+2.6 at. % Al crystal (Fig. 10) against Eq. (1) with β, T_N, γ, and D as adjustable parameters. The amplitude C_+ is obtained from the data in the paramagnetic region and C_- is calculated by an iterative procedure using Eq. (2). The critical contributions are shown as dashed curves in the insets of Figs. 7 and 10. The effect of these contributions on the fit is small, and the inclusion or deletion of the terms I_{C+} and I_{C-} does not change the resulting value of β obtained from the fits in any significant way. The results obtained for the critical exponents β and γ and for T_N, are given in Table I. In the case of the Cr+1.9 at. % Al crystal (Fig. 9) the analysis was done without inclusion of the I_{C+} and I_{C-} terms in Eq. (1) because of a lack of experimental points in the

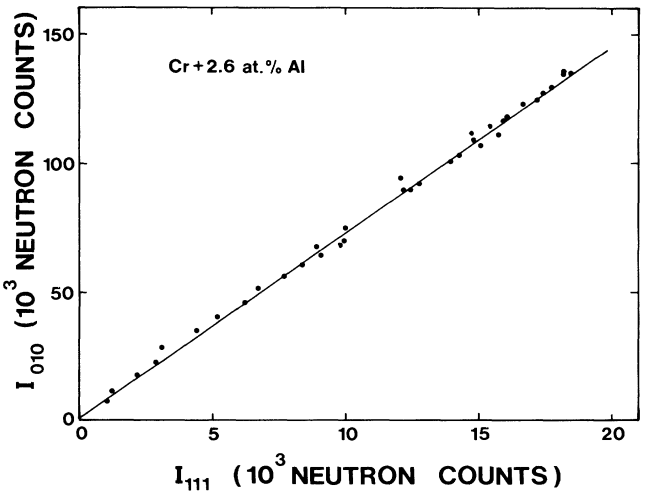

FIG. 11. Ratio of the integrated intensities of two magnetic peaks I_{010} and I_{111} for Cr+2.6 at. % Al, in the temperature range from 14 K to T_N. The linear relationship observed shows that the stronger (0,1,0) reflection does not suffer from extinction effects.

TABLE I. Critical exponents β and γ and Néel temperature T_N, found by least-squares analysis of the integrated magnetic intensities near T_N, as well as the spin-flip temperature T_{sf} deduced from neutron scattering for Cr-Al single crystals. Also indicated are values of T_N and T_{sf} deduced from elastic constant anomalies as discussed in Sec. III A.

	Cr–1.2 at. % Al	Cr–1.9 at. % Al	Cr–2.6 at. % Al
T_N (K) Neutron diffraction	219	134	256
β	0.475	0.499	0.476
γ	1.52		1.10
T_N (K) Ultrasonics	220	134	256
T_{sf} (K) Neutron diffraction	55		
T_{sf} (K) Ultrasonics	45		

paramagnetic region in this case. It is observed that the critical exponent β takes on the mean-field-like value of 0.5 for all crystals. This behavior is reflected in the clearly linear variation of the magnetic integrated intensity with temperature below T_N, covering a temperature range between $0.8T_N$ and T_N in the case of Cr+2.6 at. % Al. Similar linear behavior has been observed for Cr+0.5 at. % Fe (Ref. 26) and Cr+0.5 at. % V (Ref. 33).

IV. DISCUSSION

Walker[34] calculated the discontinuities in the elastic constants of Cr in the single-Q single-S state at T_N by using a phenomenological mean-field theory. He used the Landau approach, and his theory is valid for a continuous transition, i.e., a second-order one, at T_N. In the case of pure Cr the transition at T_N is observed[27,28] experimentally by neutron-diffraction techniques to be first order making the theory of Walker[34], strictly speaking, not applicable. As the first-order transition in Cr is very weak, Muir, Perz, and Fawcett,[23] nevertheless, applied Walker's[34] theory to pure Cr and found that the discontinuities in the elastic constants at T_N agree qualitatively with the predictions of the theory. As the present neutron-diffraction results seem to indicate that the transitions in all Cr-Al crystals are second order, they might be better suited than pure Cr for an application of Walker's[34] theory. This is particularly so for the Cr+1.2 at. % Al crystal, which shows a clear discontinuity in c_{11} at T_N of which the size could be determined fairly accurately. Furthermore, it behaves very similar to pure Cr, being in the ISDW phase for $T < T_N$ and showing a very high attenuation peak at the temperature of the discontinuity, as was also found for pure Cr by Muir, Perz, and Fawcett.[23] The situation in Cr+1.2 at. % Al is even better than in pure Cr for which the discontinuity is partially masked by the very sharp λ anomaly near T_N.

For single-Q single-S Cr, Walker[34] shows that the discontinuity at T_N in the longitudinal elastic constants c_{11}, c_{22}, and c_{33} should be positive and of equal magnitude (see also Muir, Perz, and Fawcett[23]), while the discontinuity in the shear constant c_{44} should be zero and that in the other shear constants much smaller than $\Delta c_{ii}(i=1,2,3)$. Our measurements were done on multiple-Q Cr-Al single crystals. For Cr+1.2 at. % Al we estimated from Fig. 2(a), that $\Delta c_{11}/c_{11}$ is close to +2% at T_N, which is positive as predicted by Walker[34] but smaller than the value +4% obtained by Muir, Perz, and Fawcett[23] for single-Q Cr. From Fig. 4(a) $\Delta c_{44}=0$ for Cr+1.2 at. % Al, as predicted. As $\frac{1}{2}(c_{11}-c_{12})$ does not show a clear discontinuity at T_N we used the method of Muir, Perz, and Fawcett[23] to determine $\Delta[\frac{1}{2}(c_{11}-c_{12})]$ as marked in Fig. 3(a). The value of $\Delta[\frac{1}{2}(c_{11}-c_{12})]/\frac{1}{2}(c_{11}-c_{12})$ from Fig. 3(a) is equal to about 1% which is not, as predicted, relatively small compared to $\Delta c_{11}/c_{11}$. A similar analysis was not done for the other two samples as they do not show clear discontinuities in c_{11} at T_N.

The temperature dependence of the elastic constants below T_N were analyzed using the thermodynamic model described by Fawcett,[35] which was also used by Steinemann.[36,37] In this model the magnetic free energy at low temperatures is given by

$$\Delta F(T,\omega)=\phi(\omega)f(t(\omega)) , \tag{3}$$

where $\phi(\omega)$ depends on the volume strain (ω) and $t(\omega)=T/T_0(\omega)$, $T_0(\omega)$ being a temperature parameter. By assuming $f(t)=(1-t^2)^2$,[35–37] and using Eq. (3), one obtains [see also Ref. 35 and Muir, Perz, and Fawcett (Ref. 23), who consider ϕ as a constant parameter]

$$\Delta c_{ij}(T)=\frac{\partial^2(\Delta F)}{\partial\varepsilon_i\partial\varepsilon_j}=\Delta c_{ij}(0)(1+bT^2+cT^4) ,$$

$$\Delta B(T)=\frac{\partial^2(\Delta F)}{\partial\omega^2}=\Delta B(0)(1+b_1T^2+c_1T^4) , \tag{4}$$

and

$$\Delta\omega(T)=-\frac{1}{B}\frac{\partial(\Delta F)}{\partial\omega}=\Delta\omega(0)(1+b_2T^2+c_2T^4) ,$$

where $\Delta\omega$ is the magnetovolume and the b's and c's are constants containing ϕ, its first and second derivatives to strain, and T_0 and its first and second derivatives to strain.

As shown in Figs. 2, 3, and 5 (right-hand-side plots,

dashed lines), Eq. (4) fits the results for Δc_{11}, $\Delta[1/2(c_{11}-c_{12})]$, and ΔB fairly well nearly up to T_N. The fitting parameters b, c, e, f, b_1, c_1, $\Delta c_{11}(0)$, $\Delta[\frac{1}{2}(c_{11}-c_{12})](0)$, and $\Delta B(0)$ are listed in Table II. The parameters e, f, and $\Delta[\frac{1}{2}(c_{11}-c_{12})](0)$ are contained in the corresponding equation for $\Delta[\frac{1}{2}(c_{11}-c_{12})](T)$.

The parameters b_1 and c_1 were also determined for pure Cr from the data given by Fawcett.[35] For pure Cr a near perfect fit of Eq. (4) is obtained up to 160 K with the parameters shown in Table II. b_1 is very roughly the same for Cr and the Cr-Al alloys, while c_1 varies between -0.6×10^{-10} K^{-4} and 40.4×10^{-10} K^{-4} in the concentration range of the measurements. The parameters b_1 and c_1 contain ϕ, $\phi'=d\phi/d\omega$, $\phi''=d^2\phi/d\omega^2$, and $d\ln T_0/d\omega$ [neglecting second-order derivatives of T_0 (Ref. 35)] and their experimental values can be used to determine $d\ln\phi/d\omega=\phi'/\phi$ and $d\ln T_0/d\omega$. For pure Cr we have[35]

$$\frac{1}{B(0)}\frac{\Delta B(0)}{\Delta\omega(0)}=\frac{\phi''}{\phi'}=-70$$

and using the experimentally determined b_1 and c_1 values of Table II we obtained for pure Cr, $d\ln\phi/d\omega=150$ and $d\ln T_0/d\omega=51$.

Fawcett[35] estimated $d\ln\phi/d\omega$ and $d\ln T_0/d\omega$ for pure Cr from elastic constant, thermal expansion, and specific-heat measurements at $T\rightarrow0$. He obtained $d\ln\phi/d\omega=70$ and $d\ln T_0/d\omega=25$, which are of the same order of magnitudes, but half as large, as those obtained in a different manner using the thermodynamic model with $f(t)=(1-t^2)^2$ and the experimental temperature dependence of $B(T)$. The $(1+b_1T^2+c_1T^4)$ temperature dependence of ΔB was also found experimentally in Cr-Mo-Si alloys by Smit and Alberts.[38] We also calculated $d\ln T_0/d\omega$ and $d\ln\phi/d\omega$ for the Cr-Al alloys from the b_1 and c_1 values of Table II using $\Delta\omega(0)$ values from Ref. 11 and obtained the values listed in Table II. Both $d\ln T_0/d\omega$ and $d\ln\phi/d\omega$ increase to very large values as the Al concentration is increased. The large values of these two quantities must be related to the very large dT_N/dp values of Cr-Al alloys as deduced from magnetoelastic measurements by Alberts and Lourens.[11] For the magnetovolume we have[11]

$$\Delta\omega(T)=C(T)\langle M^2(T)\rangle\ , \tag{5}$$

where the magnetoelastic coupling constant $C(T)$ is taken to be temperature dependent,

$$C(T)=C(0)[1-\xi(T/T_N)^2] \tag{6}$$

and

$$\langle M^2(T)\rangle=\langle M^2(0)\rangle[1-\alpha(T/T_N)^2+\delta(T/T_N)^4]\ , \tag{7}$$

where $\langle M^2(T)\rangle$ is the mean-square magnetic moment. This gives

$$\frac{\Delta\omega(T)}{\Delta\omega(0)}=1+A(T/T_N)^2+B(T/T_N)^4\ , \tag{8}$$

as in Eq. (4). Equation (8) fits the experimental $\Delta\omega(T)$ of polycrystalline Cr-Al alloys very well[11] with physical acceptable values for A and B, verifying the validity of the thermodynamic model for $\Delta\omega(T)$ [Eq. (4)]. Constants $A=-(\xi+\alpha)$ and $B=\delta+\alpha\xi$ were determined by Alberts and Lourens[11] from the elastic constant and thermal-expansion measurements on polycrystalline Cr-Al alloys.

Having done the neutron-diffraction measurements on the Cr-Al single crystals we are now in a position to check on Eqs. (6), (7), and (8). We did so for Cr+2.6 at.% Al, which remains in the CSDW phase down to 4 K and has a simple antiferromagnetic structure below T_N. As shown in Fig. 10 by the dashed line in the main figure, $M^2(T)/M^2(0)$, being the integrated intensity, is reasonably well fitted by Eq. (7) with $\alpha=1.00$ and $\delta=0.03$. Using these values we obtained for Cr+2.6 at.% Al, $A+B=-0.96$ and $\xi=-0.52$ (using

TABLE II. The fitting parameters from Eq. (4) for the elastic constants and bulk modulus together with fitting parameters from Eq. (7) for magnetization (α and δ) for Cr-Al alloys below T_N. Also shown are values obtained for pure Cr from the work of Fawcett (Ref. 35) as well as values of $d\ln\phi/d\omega$ and $d\ln T_0/d\omega$ determined from b_1 and c_1.

Compound Fitting Parameters	Pure Cr	Cr+1.2 at.% Al	Cr+1.9 at.% Al	Cr+2.6 at.% Al
$\Delta c_{11}(0)(10^{10}$ N m$^{-2})$		1.596	3.339	7.904
$b(10^{-6}$ K$^{-2})$		2.648	8.520	7.064
$c(10^{-10}$ K$^{-4})$		9.128	26.811	−0.755
$\Delta[\frac{1}{2}(c_{11}-c_{12})](0)$ $(10^{10}$ N m$^{-2})$			0.422	0.740
$e(10^{-6}$ K$^{-2})$			−33.177	1.016
$f(10^{-10}$ K$^{-4})$			−12.569	−2.704
$\Delta B(0)(10^{10}$ N m$^{-2})$	1.764	0.969	2.817	6.944
$b_1(10^{-6}$ K$^{-2})$	9.496	14.627	10.975	8.319
$c_1(10^{-10}$ K$^{-4})$	0.059	15.102	40.409	−0.594
α			0.76	1.00
δ			−0.23	0.03
$d\ln\phi/d\omega$	150	132	468	950
$d\ln T_0/d\omega$	51	65	196	273

$A=-0.48$ for Cr+2.74 at. % Al). For polycrystalline Cr+2.74 at. % Al Alberts and Lourens[11] obtained $A+B=-0.84$ from thermal-expansion measurements, which compares fairly well with the neutron-diffraction result. The value $\xi=-0.52$ gives an increase in $C(T)$ with increasing temperature, which seems a little surprising. Assuming the integrated intensity of the satellite for Cr+1.9 at. % Al in Fig. 9 to vary as $\langle M^2(T)\rangle/\langle M^2(0)\rangle$, we also fit Eq. (7) to the results of Fig. 9. The best fit is obtained for $\alpha=0.76$ and $\delta=-0.23$ and is fairly good as shown in Fig. 9 (broken line in the main figure). With these values we obtain $0.76A+B=-0.80$. Alberts and Lourens[11] found from thermal-expansion measurements $0.76+B=-0.48$ for Cr+1.7 at. % Al and -0.39 for Cr+2.19 at. % Al. The correspondence with the neutron work is not as good as for Cr+2.6 at. % Al and may be ascribed to the relative small values[11] of $|\Delta\omega|$ near 2 at. % Al, making the accurate determination of A and B from thermal-expansion measurements problematic. Due to the inaccuracies in A and B as determined from the thermal-expansion measurements (see Fig. 1 of Ref. 11 near 2 at. % Al), we could not determine a reliable value of ξ for the Cr +1.9 at. % Al crystal. We nevertheless conclude from the neutron-diffraction work on the Cr+2.6 at. % Al single crystal that Eq. (7) is suitable for a description of the magnetovolume in Cr-Al alloys.

The magnetic phase diagram plotted on the basis of the present results (stars) together with the previous data of Alberts and co-workers[6,10,11] is presented in Fig. 12. The hatched area is indicative of the difference between the phase diagrams obtained in previous works on polycrystalline material and the present one based on single crystals. The difference may partly be ascribed to the different techniques that were used in defining T_N. In the ultrasonic wave velocity studies on polycrystalline material T_N was defined for the ISDW samples ($c<2$ at. % Al) at the minima in the B vs T curve. The present neutron-diffraction work however indicates that T_N lies

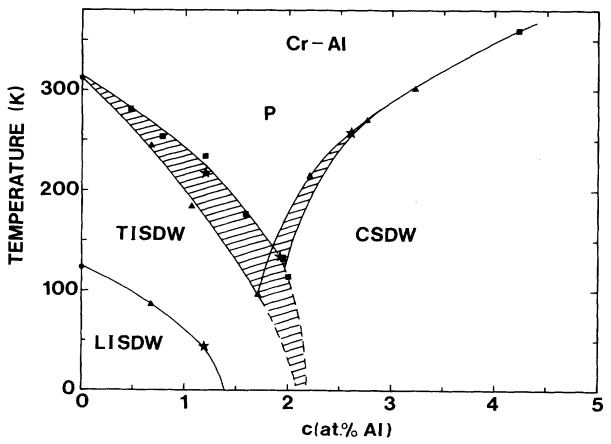

FIG. 12. Magnetic phase diagram for Cr-Al alloys proposed on the basis of our present neutron-diffraction and ultrasonic data (stars) as well as previous results of Alberts and co-workers, i.e., electrical resistivity (Ref. 6) (squares) and magnetoelastic data (Refs. 10 and 11) (triangles). The T_N and T_{sf} values for pure Cr (circles) have been taken from (Ref. 22).

to the right of the minimum points, either at the discontinuity of $c_{11}(T)$ (if such a discontinuity exists) or close to the inflection point, which defines T_N also for the CSDW samples ($c>2$ at. % Al). For instance, for the Cr+1.2 at. % Al single crystal T_N estimated in this way lies 13 K to the right of the minimum. Another contribution to this difference may result from the error in determining the Al concentration (in our case 8% of the nominal Al concentration). It cannot, however, fully explain the discrepancy marked by the hatched area, which reaches values as large as 60 K in T_N for small Al concentrations. The situation is better for Al concentrations greater than 2.5 at. %.

The neutron-diffraction results indicate that the boundary between the ISDW and the CSDW phases must be corrected in respect to that presented in Ref. 13 or in Fig. 1(a) by the dashed line, which was proposed on the basis of the Al-concentration dependence of the magnetic part of the electrical resistivity for Cr-Al alloys. This I-C boundary is probably much steeper, like that indicated in Fig. 12 by the hatched area between the broken lines. In this latter area the present experiments do not indicate any mixed ISDW and CSDW phases as previously suggested.[7,8,11,12] Furthermore, we were able to add another point to the LISDW-TISDW phase boundary, which seems to drop to zero for a smaller Al concentration than previously anticipated [compare with Fig. 1(a)].

V. CONCLUSIONS

Concerning the discrepancy in the position of the minimum on the magnetic phase diagram mentioned in the Introduction, our present results confirm the previous results of Alberts and co-workers[6,10,11] that this minimum occurs at higher values of the Al content ($1.7\le c\le 2.0$ at. % Al) and lower Néel temperature ($100\le T_N\le 140$ K) than that obtained by Arajs and co-workers[3,5] and more recently by Yakhmi *et al.*,[7] who placed this minimum at $1.0\le c\le 1.2$ at. % Al and $170\le T_N\le 200$ K [see Fig. 1(b)]. This discrepancy is mainly caused by data published for Cr+1.9 at. % Al for which the Néel temperature is reported by Yakhmi[7] as equal to 240 K and by Arajs[3,5] as 310 K, whereas the value for our two independent samples (one polycrystalline and one single crystalline) is equal to only 130 K.

The magnetic phase diagram reported by Chakrabarti and Beck[4] not necessarily contradicts ours, since their work lacks data in the controversial concentration region $1.2\le c\le 2.5$ at. % Al (Ref. 4) [see Fig. 1(b)]. Also the phase diagram presented by Sousa *et al.*[8] seems to be in agreement with ours, except for the T_N value reported for Cr+2.83 at. % Al [see Fig. 1(b)], which was in our opinion wrongly interpreted as being indicated by the $\chi(T)$ low-temperature anomaly at 25 K instead of by the high-temperature one at about 250 K (for details see Ref. 8). We plotted the temperatures of both anomalies in Fig. 1(b) [dashed-dotted line in Fig. 1(b)].

As regards to the boundary between the ISDW and CSDW phases on the magnetic phase diagram we found no evidence of either a transition from the ISDW to CSDW phase or for the coexistence of these phases

within any of our samples Cr+1.2, 1.9, and 2.6 at. % Al. Samples Cr+1.2 and 1.9 at. % Al remain in the ISDW state at all $T < T_N$ whereas the Cr+2.6 at. % Al remains in the CSDW state at $T < T_N$. The I-C boundary line runs probably steeply in the vicinity of 2.0% Al. It should be mentioned that the neutron-diffraction results by Mizuki, Endoh, and Ishikawa[16] show that Cr+1.9 at. % Al remains in the CSDW phase at all $T < T_N$ in contradiction with our results. It is then very likely that the I-C phase boundary is very steep and that small differences in the Al composition around 1.9 at. % Al, or small errors in the determination of the Al concentration in this region, may place the sample on either side of I-C boundary. It will therefore be a difficult task to prepare a sample that shows an I-C transition.

The neutron-diffraction studies show second-order phase changes at T_N in all three Cr-Al crystals studied.

The temperature dependence of the elastic constants is described fairly well by the thermodynamic model. The magnetic contribution for $\frac{1}{2}(c_{11}-c_{12})$ at T_N for Cr+1.2 at. % Al is of the same order of magnitude as that for c_{11}, in contrast with the predictions of Walker's[34] theory. However, $\Delta c_{44}=0$ at T_N, as predicted by theory.

The magnetization $M^2(T)/M^2(0)$ of Cr+1.9 at. % Al nd Cr+2.6 at. % Al for $T < T_N$, varies as $[1-\alpha(T/T_N)^2+\delta(T/T_N)^4]$. The values of α and δ compare fairly well with the results of magnetovolume data. This in a sense verifies the use of the term $f(t)=(1-t^2)^2$ in the magnetic free energy of the thermodynamic model.

ACKNOWLEDGMENTS

Financial aid from the South African Foundation for Research Development and from the Atomic Energy Corporation of South Africa (Ltd) is gratefully acknowledged, as well as technical help from S. I. Wagener in growing the single crystals.

*On leave from Institute of Low Temperature and Structure Research, P.O. Box 937, 50-950 Wroclaw, Poland.

[1]A. Arrott, in *Magnetism,* edited by G. T. Rado and H. Suhl (Academic, New York, 1966), Vol. II B.

[2]E. Fawcett, Rev. Mod. Phys. **60**, 209 (1988).

[3]S. Arajs, K. V. Rao, H. U. Åström, and T. F. De Young, Phys. Scr. **8**, 109 (1973).

[4]D. J. Chakrabarti and P. A. Beck, J. Phys. Chem. Solids **32**, 1609 (1971).

[5]S. Arajs, N. L. Reeves, and E. E. Anderson, J. Appl. Phys. **42**, 1691 (1971).

[6]H. L. Alberts and S. J. Burger, Solid State Commun. **28**, 771 (1978).

[7]J. V. Yakhmi, I. K. Gapalakrishnan, R. M. Iyer, and J. L. Stanford, J. Appl. Phys. **61**, 3994 (1987).

[8]J. B. Sousa, M. M. Amado, R. P. Pinto, M. F. Pinheiro, M. E. Braga, J. M. Moreira, L. E. Hedman, H. U. Åström, L. Khlaif, P. Walker, G. Garton, and D. Hukin, J. Phys. F **10**, 2535 (1980).

[9]I. Pop, D. Dadârlat, T. Petrisor, and A. Giurgiu, J. Phys. Chem. Solids **42**, 927 (1981).

[10]H. L. Alberts and J. A. J. Lourens, J. Magn. Magn. Mater. **31-34**, 131 (1983).

[11]H. L. Alberts and J. A. J. Lourens, Phys. Rev. B **29**, 5279 (1984).

[12]A. Kallel and F. De Bergevin, Solid State Commun. **5**, 955 (1967).

[13]H. L. Alberts, J. Phys. F **15**, L171 (1985).

[14]M. A. Lind and J. L. Stanford, J. Phys. Soc. Jpn. **53**, 4029 (1984).

[15]K. Mikke and J. Jankowska, in *Proceedings of the International Conference on the Physics of Transition Metals, Toronto, 1977,* edited by M. J. G. Lee, J. M. Perz, and E. Fawcett (IOP, London, 1978), Chap. 7.

[16]J. Mizuki, Y. Endoh, and Y. Ishikawa, J. Phys. Soc. Jpn. **51**, 3497 (1982).

[17]H. L. Alberts, J. Phys.: Condens. Matter **1**, 4993 (1989).

[18]S. A. Werner, A. Arrott, and H. Kendrick, Phys. Rev. **155**, 528 (1967).

[19]M. Bohlmann and H. L. Alberts, J. Phys. E **3**, 779 (1970).

[20]H. L. Alberts, J. Phys.: Condens. Matter **2**, 9707 (1990).

[21]R. B. Roberts, G. K. White, and E. Fawcett, Physica (Utrecht) **119B**, 63 (1983).

[22]H. J. van Rijn and H. L. Alberts, J. Phys. F **13**, 1559 (1983).

[23]W. C. Muir, J. M. Perz, and E. Fawcett, J. Phys. F **17**, 2431 (1987).

[24]K. W. Katahara, M. Nimalendran, M. H. Manghnani, and E. S. Fisher, J. Phys. F **9**, 2167 (1979).

[25]T. J. Bastow and R. Street, Phys. Rev. **141**, 510 (1966).

[26]A. Arrott, S. A. Werner, and H. Hendrick, Phys. Rev. **153**, 624 (1967).

[27]A. Arrott, S. A. Werner, and H. Kendrick, Phys. Rev. Lett. **14**, 1022 (1965).

[28]H. Betsuyaku, Phys. Rev. Lett. **42**, 536 (1979).

[29]Y. Ishikawa, S. Hoshino, and Y. Endoh, J. Phys. Soc. Jpn. **22**, 1221 (1967).

[30]G. E. Bacon, *Neutron Diffraction,* 3rd ed. (Clarendon, Oxford, 1975), Chap. 3.1.

[31]H. E. Stanley, *Phase Transitions and Critical Phenomena* (Clarendon, Oxford, 1971).

[32]P. Schofield, J. D. Lister, and J. T. Ho, Phys. Rev. Lett. **23**, 1098 (1969).

[33]D. R. Noakes, T. M. Holden, P. C. de Camargo, E. Fawcett, and P. de V. du Plessis, J. Appl. Phys. **64**, 5883 (1988).

[34]M. B. Walker, Phys. Rev. B **22**, 1338 (1980).

[35]E. Fawcett, J. Phys.: Condens. Matter **1**, 203 (1989).

[36]S. G. Steinemann, J. Magn. Magn. Mater. **7**, 84 (1978).

[37]S. G. Steinemann, J. Magn. Magn. Mater. **12**, 191 (1979).

[38]P. Smit and H. L. Alberts (private communication).